Available online at www.sciencedirect.com

ScienceDirect

Geochimica et Cosmochimica Acta 235 (2018) 237–245

Geochimica et Cosmochimica Acta

www.elsevier.com/locate/gca

# Theoretical calibration of the triple oxygen isotope thermometer

Justin Hayles [a,b,*], Caihong Gao [c], Xiaobin Cao [b], Yun Liu [c], Huiming Bao [b]

[a] Department of Earth, Environmental and Planetary Sciences, Rice University, United States
[b] Department of Geology and Geophysics, Louisiana State University, United States
[c] State Key Laboratory of Ore Deposit Geochemistry, Institute of Geochemistry, Chinese Academy of Sciences, China

Received 26 July 2017; accepted in revised form 29 May 2018; Available online 6 June 2018

**Abstract**

The field of isotope geochemistry began with the study of oxygen isotope geothermometry, most notably for carbonates. For traditional oxygen isotope geothermometry only the relationship between one rare isotope, oxygen-18, and the common isotope, oxygen-16, is used because for most terrestrial processes the $^{17}O$-$^{16}O$ relationship scales with the $^{18}O$-$^{16}O$ relationship and is thought to not grant any new information. However, theoretical analysis predicts a small temperature-dependence of the equilibrium triple oxygen isotope relationship and instrumentation and techniques now allow for high-precision determination of the oxygen isotope composition for all three oxygen isotopes for a variety of sample types. To set the groundwork for triple oxygen isotope geothermometry, here we present new calibrations based on statistical thermodynamics and density functional theory for both the traditional two isotope and the recently introduced triple isotope thermometer for pairs of quartz, calcite, dolomite, fluorapatite, hematite, magnetite and liquid water. The results compare well with previous studies on $^{18}O/^{16}O$ fractionation where theoretical and experimental data are available. Of the models given here, pairs of quartz, calcite, dolomite and fluorapatite with water, hematite or magnetite show promising temperature sensitivities as triple isotope thermometers with acceptable uncertainties for surface and low-T hydrothermal environments.


*Keywords:* Mineral-water equilibrium; Oxygen isotope equilibrium; Geothermometer; Triple-oxygen; $\Delta^{17}O$

## 1. INTRODUCTION

The potential for isotope fractionation to be used as a geothermometer dates back to the work of Harold Urey who recognized the temperature dependence of oxygen isotope fractionation between carbonate and water (Urey, 1947). At the time, isotope ratio mass spectrometry was in its infancy and precisions of only one part per thousand were possible for the ratio of the two most abundant isotopes of oxygen, $^{16}O$ and $^{18}O$. For low temperatures, this precision allowed for the carbonate geothermometer, with assumptions on the isotope composition of the water (Urey, 1947). Early on, it was assumed that isotope fractionation for the $^{17}O$-$^{16}O$ system would scale with $^{18}O$-$^{16}O$ system due to the mass dependent isotope fractionation (Clayton et al., 1973) and so it was thought that measuring the $^{17}O/^{16}O$ ratio would provide no useful further information. The discovery of $^{17}O$ deviation in meteorites from the terrestrial fractionation line and later large non-mass-dependent isotope effects associated with ozone chemistry in Earth's atmosphere changed this paradigm and led to a newfound need in measuring the triple isotope composition of various oxygen reservoirs (Clayton et al., 1973; Heidenreich and Thiemens, 1983; Thiemens, 2013). Over time, analytical precision and techniques improved to the point where much smaller mass-dependent variations are resolvable and can be related to chemically and geochemically relevant parameters (Pack and Herwartz, 2014; Liang and Mahata, 2015; Bao et al., 2016; Sharp et al., 2016). What has become apparent is that much like with

* Corresponding author at: Department of Earth, Environmental and Planetary Sciences, Rice University, United States.
*E-mail address:* justin.a.hayles@rice.edu (J. Hayles).

https://doi.org/10.1016/j.gca.2018.05.032
0016-7037/

the two isotope systems, fractionation in triple isotope systems is temperature dependent (Cao and Liu, 2011; Pack and Herwartz, 2014; Bao et al., 2016; Hayles et al., 2017). This extra dimension of temperature dependency led to the suggestion by Pack and Herwartz (2014) that the value of the mass dependence exponent, θ, can be used as a separate geothermometer for low temperature systems.

For the oxygen triple isotope system, θ is given by;

$$\theta = \frac{ln^{17}\alpha_{A-B}}{ln^{18}\alpha_{A-B}} \quad (1)$$

where α is the fractionation factor which for measurement purposes is given by:

$$^{18}\alpha_{A-B} = \frac{^{18}\beta_A}{^{18}\beta_B} = \frac{[^{18}n/^{16}n]_A}{[^{18}n/^{16}n]_B} \quad (2)$$

where $[^{18}n/^{16}n]$ is the molar ratio of the rare/heavy isotope $^{18}O$ and the common/light isotope $^{16}O$, which can be measured relative to a standard and β is a theoretical parameter relating to a hypothetical equilibrium between the phase in question and an oxygen species with no thermodynamic bias for one oxygen isotope over another. β is therefore a theoretical parameter which describes the "affinity" of a species for one oxygen isotope relative to another. In both equations, the superscript indicates the isotope system and the subscript indicates the species involved in equilibrium (e.g. A-B => Calcite-$H_2O_{(L)}$).

Not long after the introduction of the θ based triple isotope thermometer, the concept of using the temperature dependence of the difference in $\Delta'^{17}O$ between minerals and water as a geothermometer was introduced. This was independently suggested by Bao et al. (2016) based on previous theoretical work for calcite-water equilibrium and Sharp et al. (2016) based on measurements of natural quartz and silica. The core concept of $\Delta'^{17}O$ is given by the equation:

$$\Delta'^{17}O = \delta'^{17}O - 0.5305\delta'^{18}O \quad (3)$$

where *isgivenby* :is given by:

$$\delta'^{18}O = ln\frac{[^{18}n/^{16}n]_{sample}}{[^{18}n/^{16}n]_{standard}} \quad (4)$$

Using Eqs. (2) and (4), the difference on $\delta'^{18}O$ (or $\Delta\delta^{18}O$) between two phases given by;

$$\Delta\delta'^{18}O_{A-B} = ln^{18}\alpha_{A-B} \quad (5)$$

The similar expression for the difference in $\Delta'^{17}O$ (or $\Delta\Delta^{17}O$) between two phases is then given by;

$$\Delta\Delta'^{17}O = \Delta\delta'^{17}O - 0.5305\Delta\delta'^{18}O \quad (6)$$

Based on prior use (Pack and Herwartz, 2014; Wiechert et al., 2004) as well as the arguments put forth by Hayles et al. (2017) and Bao et al. (2016), here the suggested 0.5305 is used for Eqs. (3) and (6) as opposed to other commonly used values (e.g. 0.52, 0.528). This value is very nearly equal to the high-temperature limit of θ for oxygen isotope fractionation under the harmonic approximation and allows for a monotonic, or very near monotonic behavior for the temperature dependence of $\Delta\Delta'^{17}O$.

Although mathematically equivalent, in practice, the use of $\Delta\Delta'^{17}O$ has three primary advantages over the use of θ. (1) Application of simple the $\Delta'^{17}O$ thermometer is similar in practice to the commonly used $\delta^{18}O$ thermometer. (2) Covariance between the measurements of $\delta'^{18}O$ and $\delta'^{17}O$ lead to a higher precision for $\Delta'^{17}O$ than would be expected from the uncertainties of $\delta'^{18}O$ and $\delta'^{17}O$. (3) The temperature dependency of $\Delta\Delta'^{17}O$ is simple and does not deviate from a finite range for small values of $\Delta\delta'^{18}O$. This is as opposed to θ which can be very uncertain and fundamentally hold any value for small enough values of $\Delta\delta'^{18}O$ (Hayles et al., 2017).

Sharp et al. (2016) empirically calibrated the $SiO_2$-$H_2O$ system and compared to natural samples. A sound interpretation, however, would first require the confirmation of the mineral-water equilibrium, for which a reliable theoretical calibration of both α and θ variability with T is a prerequisite. Furthermore, to extend triple oxygen isotope thermometer to the diverse mineral assemblages in surface-temperature or hydrothermal systems, we need equilibrium θ-T or $\Delta\Delta'^{17}O$-T relationships for many other common oxygen-bearing minerals. At this time, however, we only have theoretical predictions for quartz and calcite without the needed models at the same level of theory for liquid water (Cao and Liu, 2011; Hill et al., 2014).

Therefore, in this study we investigate the viability of a triple isotope thermometer based on the $^{16}O$-$^{17}O$-$^{18}O$ system from a theoretical perspective. Here the temperature dependency of $\Delta\Delta'^{17}O$ (Bao et al., 2016; Sharp et al., 2016) is used as a mass-dependent fractionation descriptor for its ease of use. New theoretical calculations for equilibrium pairs of hematite, magnetite, fluorapatite, calcite, dolomite, quartz and liquid water and water vapor were carried out for both the $\delta'^{18}O$ and $\Delta'^{17}O$ systems. The structures for minerals and liquid water are represented by molecular clusters, and the Volume Variable Cluster Method is adopted here to allow for optimizing the structures for minerals at different theoretical levels (Li and Liu, 2015). It is found that using the assumption of isotope equilibrium: fluorapatite-$H_2O_{(L)}$, calcite-$H_2O_{(L)}$, dolomite-$H_2O_{(L)}$, and quartz-$H_2O_{(L)}$ can be effective triple isotope thermometers for surface to hydrothermal environments. Both hematite and magnetite can be used in place of $H_2O_{(L)}$ for the above pairs with only minor reduction in temperature sensitivity.

## 2. METHODS

### 2.1. Calculation of $\beta_h$ for minerals

Periodic boundary conditions are typically used to represent the crystal environment and have been used to predict inter-minerals isotope fractionation factors for many systems (Schauble, 2011; Huang et al., 2013). However, this method is challenged when dealing with systems involving aqueous species. In order to use consistent methods for the representation of both minerals and aqueous species, molecule-like clusters were introduced to predict mineral-aqueous isotope fractionation factors (Gibbs, 1982;

Rustad et al., 2010). Cao and Liu (2011) employed small cluster models to investigate theta values for calcite-water and quartz-water pairs (Cao and Liu, 2011). However, their cluster models, particularly for calcite, were too small to be expected to generate accurate fractionation values. Although smaller clusters do generate approximate results, in general, larger clusters will produce more accurate results because the chemical/crystal environment simulated by larger cluster better simulates what is expected in a real system. This would make the previous results less accurate than the current models for mineral-water equilibrium at a given level of theory.

Here, the Volume Variable Cluster Method (Li and Liu, 2015) is used for the calculation of values of β under the harmonic approximation ($\beta_h$) for all minerals. VVCM is similar to the embedded cluster method (Rustad et al., 2010). The original mineral structures are taken from American Mineralogist Crystal Structure Database (Downs and Hall-Wallace, 2003). The modeled clusters are cut from these mineral structures with the atoms of interest (e.g. O-atoms or $PO_4$ groups) at the core. For example, if the O or C atoms in carbonate minerals are of interest, a $CO_3$ group is placed at the core of the clusters and surrounded by six metal atoms as the second shell, the third shell is made of $CO_3$ with the O atoms at the edge. As with any cluster model, ideally larger clusters would be used, but computation costs increase exponentially with each additional shell. Cluster size may have effects on the frequencies and therefore the value of $\beta_h$, but isotope effects are dominantly local to the substituted atom and each subsequent shell has a diminishing influence on $\beta_h$ at an increasingly significant computational cost. To test the influence of cluster size, two cluster sizes are tested for quartz, the least computationally costly mineral investigated.

In order to maintain a neutral environment for the modeled clusters, hundreds of virtual point charges are added at the edge of clusters by bonding to the outer O atoms at certain bond lengths. Rustad et al. (2010) suggested an embedded cluster method with outermost point charges bond to outer fixed O atoms at a distance of 1 Å, however, this distance may significantly influence the $\beta_h$ values.

In our model scheme, the outermost virtual point charges may have different valences which are determined by the bonding environment. For example, in the calcite cluster model, there are 48 point charges each with a valence of 1/6, these charges are bound to the bridging O which connects the Ca atom and outer C atom. There are another 81 point charges each with a valence of 2/9, these point charges are bond to the outer O atoms. In our model scheme, the point charges are fixed at different distances, and the full-cluster is optimized accordingly to locate the most stable configuration. The calcite cluster has two kinds of point charges, so the searching procedure is conducted twice to find the optimal distance for each. The point charges are adjusted in increments of 0.01 Å. As a result of this, we provide that the optimal point charge distance may differ from the chosen value by this degree. An analysis of the uncertainty associated with this variation on the calculated values is provided in of the supplemental information.

Once optimal point charge distances are found, the clusters are optimized, the outer atoms are fixed to avoid contamination by rotational and translational degrees of freedom and the harmonic frequencies are calculated using GAUSSIAN09 (Frisch et al., 2016) to the B3LYP/6-311g (d) level of theory for all minerals including the larger quartz cluster. As a test of the sensitivity to the basis set, the smaller quartz cluster model is also calculated to the B3LYP/6-311 g+ (2df, p) level of theory. $\beta_h$ values are calculated from the resulting harmonic frequencies through application of the B-GM-U model (Bigeleisen and Goeppert-Mayer, 1947; Urey, 1947):

$$\beta_h^* = \prod_i^{3n-6(5)} \left(\frac{u_i^*}{u_i}\right)_{TRPR} \left(\frac{e^{-u_i^*/2}}{e^{-u_i/2}}\right)_{ZPE} \left(\frac{1-e^{-u_i}}{1-e^{-u_i^*}}\right)_{EXC} \quad (7)$$

$$u^* = \frac{h\upsilon^*}{k_B T} \quad (8)$$

where υ is the vibrational frequency of an individual degree of freedom and "*" indicates parameters relating to the heavy isotope (i.e. $^{17}O$ or $^{18}O$). Eq. (7) is equivalent to a ratio of the quantum contributions to the vibrational partition functions for the heavy substituted and non-substituted isotopologues. Other contributions effectively cancel when the ratio of partition functions are taken for different isotopologues for the same molecule. The exceptions to this can be found at particularly low temperatures where rotation may deviate from classical behavior and for molecules which contain hydrogen where anharmonic effects become significant. All calculations of $\beta_h$ from frequencies are conducted in R (R Core Team, 2012).

### 2.2. Calculation of $\beta_h$ for liquid water

The primary difficulty in modeling liquid water for the purposes of isotope fractionation calculations is the need to incorporate anharmonic correction terms to achieve accurate $\beta_h$ values. Currently there is not a good solution for liquid water to be accurate enough for our purposes. Fortunately, isotope fractionation between water vapor and liquid water has been well studied experimentally to good precision and sufficiently accurate anharmonic corrections are possible for water vapor. Anharmonically corrected $^{18}\beta$ values for liquid water are calculated using $^{18}\alpha_{H2O(l)\text{-}H2O(v)}$ values from a best fit curve given by Horita et al. (2008). The empirical best fit $^{18}\alpha_{H2O(l)\text{-}H2O(v)}$ values are multiplied by calculated $^{18}\beta$ values for a lone water molecule which accurately represents water vapor under most conditions. The $^{18}\beta$ values for water vapor include the anharmonic correction to zero point energy and are calculated at the B3LYP/6-311g (d) and B3LYP/6-311g+ (2df, p) levels of theory corresponding to the appropriate mineral models. By addressing liquid water in this way, contributions from the anharmonic correction as well as configurational disorder of liquid water (e.g. non tetrahedral coordination of some waters, transient hydrogen bonds, etc.) are considered for $^{18}O$-$^{16}O$ fractionations.

Experimental work has been done on the equilibrium triple oxygen isotope relationship between liquid water

and water vapor (Barkan and Luz, 2005), but data are sparse. For this reason, κ (= $ln^{17}\beta/ln^{18}\beta$) values for liquid water must be theoretically calculated. This is addressed by generating a theoretical model for $H_2O_{(l)}$-$H2O_{(v)}$ triple oxygen isotope equilibrium which does not include the anharmonic correction. Based on the assumption that the anharmonic corrections to liquid water and water vapor follow a similar mass dependency, this method will more accurately reflect real $H_2O_{(l)}$-$H_2O_{(v)}$ equilibrium values due to partial cancelation. For κ, the anharmonic correction is small because any anharmonic contribution to κ follows a similar mass dependency to harmonic contributions with the effect scaling with correction's fractional contribution to ln(β) which is typically on the order of a few percent for hydrogen bearing molecules (Cao and Liu, 2011; Hayles et al., 2017). Because of this and owing to the previously identified cancelation of errors in calculations of isotope fractionation using the harmonic model, a slight inaccuracy in this assumption is expected to have a minimal impact on the calculated value of κ (Webb and Miller, 2014). This procedure, however, does not consider the configurational disorder of liquid water.

The theoretical liquid water model for κ consists of eleven cluster models with different initial geometries. Each water cluster consists of twenty two water molecules arranged and optimized to the B3LYP/6-311g (d) and B3LYP/6-311+g*(2df,p) levels of theory. Individual $^{17}\beta_h$ and $^{18}\beta_h$ values from substitutions of each water molecule in the cluster are calculated using the B-GM-U model and the results are averaged to give β values for that cluster. The results of these models are combined with the results from a non-anharmonically corrected water vapor model calculated at the same level of theory to determine theoretical values for $^{18}\alpha_{H2O(l)\text{-}H2O(v)}$ and θ to the harmonic approximation. The resulting $\ln(^{18}\alpha_{H2O(l)\text{-}H2O(v)})$ are increasingly higher than the experimental results with increasing temperature but stay within 1‰ of the experimental results up to about 200 °C. This is likely due to the increasing importance of dimers and trimers in the structure of water vapor at higher temperatures, but may also relate to differences in the structure of liquid water (Driesner and Seward, 2000). The resulting theoretical $\theta_{H2O(l)\text{-}H2O(v)}$ values agree with the values given by Barkan and Luz (2005) of 0.529 ± 0.001 for 11.4 °C to 41.5 °C. The theoretical $\theta_{H2O(l)\text{-}H2O(v)}$ values are paired with the experimental vapor-liquid equilibrium results to calculate semi-empirical $^{17}\alpha_{H2O(l)\text{-}H2O(v)}$ values which are in turn used to calculate $^{17}\beta_{H2O(l)}$ values the same manner as was done for $^{18}\beta_{H2O(l)}$ and κ values using the equation:

$$\kappa = \frac{ln^{17}\beta}{ln^{18}\beta} \tag{9}$$

## 3. RESULTS

Rather than reporting functions for $\ln(^{18}\alpha)$ and θ values as is typical, here high order polynomial fits to functions of 1/T are reported for $\ln(^{18}\beta)$ and κ (Tables 1 and 2). These can be converted to $^{18}\alpha$ and θ values using the equations:

Table 1
Parameters of fitting functions for $\ln(^{18}\beta)$. The fitting function is a seventh order polynomial: $\frac{A}{T^4} + \frac{B}{T^3} + \frac{C}{T^2} + \ldots + Int.$

| Material | Basis set | Other Notes | A | B | C | D | E | F | G | Intercept |
|---|---|---|---|---|---|---|---|---|---|---|
| Quartz | 6-311g (d) | | 6.994407E+14 | −1.741758E+13 | 1.712542E+11 | −7.578863E+08 | 4.188956E+05 | 1.199452E+04 | 6.306557E−02 | −2.121188E−06 |
| Quartz | 6-311g (d) | Large cluster | 7.404582E+14 | −1.829412E+13 | 1.780875E+11 | −7.773202E+08 | 3.984628E+05 | 1.220543E+04 | 3.531345E−02 | 4.923486E−06 |
| Quartz | 6-311+g*(2df,p) | | 7.195674E+14 | −1.785923E+13 | 1.748748E+11 | −7.695902E+08 | 4.124265E+05 | 1.214285E+04 | 5.186833E−02 | 7.885565E−07 |
| Calcite | 6-311g (d) | | 7.027321E+14 | −1.633009E+13 | 1.463936E+11 | −5.417531E+08 | −4.495755E + 05 | 1.307870E+04 | −5.393675E−01 | 1.331245E−04 |
| Dolomite | 6-311g (d) | | 6.981231E+14 | −1.625341E+13 | 1.461088E+11 | −5.437285E+08 | −4.352597E+05 | 1.320284E+04 | −5.279219E−01 | 1.304577E−04 |
| Apatite | 6-311g (d) | | 3.883147E+14 | −1.019859E+13 | 1.071744E+11 | −5.178151E+08 | 3.720681E+05 | 9.620602E+03 | 1.304843E−01 | −2.288222E−05 |
| Hematite | 6-311g (d) | | −7.167765E+12 | −2.951284E+11 | 1.062800E+10 | −1.048585E+08 | 6.944175E+04 | 6.729440E+03 | 4.165579E−02 | −9.221687E−06 |
| Magnetite | 6-311g (d) | | −2.441011E+12 | −4.218924E+11 | 1.194292E+10 | −1.108714E+08 | 7.569706E+04 | 6.761516E+03 | 4.468434E−02 | −9.842431E−06 |
| Liquid water | 6-311g (d) | Semi-empirical | −5.324090E+14 | 1.318367E+13 | −1.428610E+11 | 8.761135E+08 | −2.952406E+06 | 6.057270E+03 | 1.764688E+01 | −1.168952E−02 |
| Liquid water | 6-311+g*(2df,p) | Semi-empirical | −4.399381E+14 | 1.089998E+13 | −1.188669E+11 | 7.377083E+08 | −2.483798E+06 | 5.147823E+03 | 1.849064E+01 | −1.191534E−02 |
| Liquid water | 6-311g (d) | | −6.705843E+15 | 1.333519E+14 | −1.114055E+12 | 5.090782E+09 | −1.353889E+07 | 2.143196E+04 | 5.689300E+00 | −7.839005E−03 |
| Liquid water | 6-311+g*(2df,p) | | −2.355545E+15 | 5.635194E+13 | −5.610920E+11 | 3.022313E+09 | −9.629956E+06 | 1.946348E+04 | 1.601845E+00 | −6.915360E−04 |
| Water vapor | 6-311g (d) | | −2.336556E+15 | 5.574880E+13 | −5.536580E+11 | 2.973834E+09 | −9.397828E+06 | 1.775185E+04 | 3.077906E+00 | −1.032919E−03 |
| Water vapor | 6-311+g*(2df,p) | | −2.345138E+15 | 5.569138E+13 | −5.498637E+11 | 2.932679E+09 | −9.195770E+06 | 1.725555E+04 | 3.587121E+00 | −1.151189E−03 |
| Water vapor | 6-311g (d) | Anh. corrected | −2.336556E+15 | 5.574880E+13 | −5.536580E+11 | 2.973834E+09 | −9.397828E+06 | 1.775185E+04 | 2.323153E+00 | −1.032919E−03 |
| Water vapor | 6-311+g*(2df,p) | Anh. corrected | −2.345138E+15 | 5.569138E+13 | −5.498637E+11 | 2.932679E+09 | −9.195770E+06 | 1.725555E+04 | 2.833605E+00 | −1.151189E−03 |

Table 2
Parameters of fitting functions for κ. The fitting function is a fifth order polynomial: $\frac{A}{T^6}+\frac{B}{T^4}+\frac{C}{T^3}+\ldots+Int.$

| Material | Basis set | Other Notes | A | B | C | D | E | Intercept |
|---|---|---|---|---|---|---|---|---|
| Quartz | 6-311g (d) | | 7.818124E+08 | −1.907991E+07 | 1.729920E+05 | −6.526428E+02 | 2.049672E−01 | 0.5304671 |
| Quartz | 6-311 g (d) | Large cluster | 8.622466E+08 | −2.058061E+07 | 1.830413E+05 | −6.785610E+02 | 2.143374E−01 | 0.5304652 |
| Quartz | 6-311+g*(2df,p) | | 8.189887E+08 | −1.977992E+07 | 1.777741E+05 | −6.655203E+02 | 2.094910E−01 | 0.5304655 |
| Calcite | 6-311g (d) | | 1.019124E+09 | −2.117501E+07 | 1.686453E+05 | −5.784679E+02 | 1.489666E−01 | 0.5304852 |
| Dolomite | 6-311g (d) | | 9.937692E+08 | −2.069620E+07 | 1.653613E+05 | −5.704833E+02 | 1.462601E−01 | 0.5304874 |
| Apatite | 6-311g (d) | | 3.082126E+08 | −9.581022E+06 | 1.035166E+05 | −4.528486E+02 | 1.324485E−01 | 0.5304829 |
| Hematite | 6-311g (d) | | −1.363074E+08 | 1.581277E+06 | 5.389889E+03 | −1.329602E+02 | 9.865876E−03 | 0.5305161 |
| Magnetite | 6-311g (d) | | −1.378554E+08 | 1.454849E+06 | 7.483793E+03 | −1.417244E+02 | 1.307108E-02 | 0.5305117 |
| Liquid water | 6-311g (d) | Semi-empirical | −2.993068E+08 | 6.507712E+06 | −5.962566E+04 | 2.676809E+02 | −7.097807E−01 | 0.5308002 |
| Liquid water | 6-311+g*(2df,p) | Semi-empirical | −1.728419E+08 | 4.377646E+06 | −4.505342E+04 | 2.197520E+02 | −6.251547E−01 | 0.5307424 |
| Liquid water | 6-311g (d) | | 7.625734E+06 | 1.216102E+06 | −2.135774E+04 | 1.323782E+02 | −4.931630E−01 | 0.5306551 |
| Liquid water | 6-311+g*(2df,p) | | −6.800017E+07 | 2.496067E+06 | −2.983001E+04 | 1.618269E+02 | −5.159181E−01 | 0.5306614 |
| Water vapor | 6-311g (d) | | −1.999657E+08 | 4.683020E+06 | −4.397813E+04 | 2.127461E+02 | −5.622800E−01 | 0.5306689 |
| Water vapor | 6-311+g*(2df,p) | | −2.629007E+08 | 5.698243E+06 | −4.988832E+04 | 2.269539E+02 | −5.716023E−01 | 0.5306672 |
| Water vapor | 6-311g (d) | Anh. corrected | −2.678023E+08 | 5.863778E+06 | −5.193191E+04 | 2.389870E+02 | −6.063747E−01 | 0.5306843 |
| Water vapor | 6-311+g*(2df,p) | Anh. corrected | −3.282456E+08 | 6.834447E+06 | −5.752732E+04 | 2.520748E+02 | −6.136326E−01 | 0.5306809 |

$$\alpha_{A-B}=\frac{\beta_A}{\beta_B} \tag{10}$$

and,

$$\theta=\kappa_A+(\kappa_A-\kappa_B)\frac{ln\beta_B^*}{ln\alpha_{A-B}^*} \tag{11}$$

Fits to these parameters are used in order to avoid complications with crossover scenarios which are exhibited for all mineral-water exchange models given here at some temperature. The fits presented here are accurate to the models for temperatures ranging from −100 °C to 1400 °C except for the water models which are constrained by experimental results from Horita et al. (2008). The standard deviation of the residuals for all seventh-order polynomial fits to $\ln(^{18}\beta)$ is $5\times10^{-6}$ or smaller which amounts to a precision of the fits to 0.005 or better for $1000\ln(^{18}\alpha)$. The standard deviation of the residuals for the fifth-order polynomial fits for κ of liquid water is the largest at $4.5\times10^{-6}$ with other fits having standard deviations one to two magnitudes smaller. Precision of the fits to the models was the only factor in choosing polynomial order.

## 4. DISCUSSION

### 4.1. Mineral pairs with $H_2O_{(L)}$

By far, the most common application of oxygen isotope geothermometers relates to equilibrium between minerals and liquid water. The most common mineral-$H_2O_{(L)}$ thermometers utilize carbonate minerals, but geothermometers have been proposed using silicate and phosphate minerals as well (Longinel and Nuti, 1973; Lecuyer et al., 2013; Pack and Herwartz, 2014; Sharp et al., 2016). Fig. 1 illustrates the theoretical relationship between $\Delta\delta'^{18}O$ (=1000‰$\ln(^{18}\alpha)$) and temperature (Fig. 1a) as well as $\Delta\Delta'^{17}O$ and temperature (Fig. 1b) for mineral-$H_2O_{(L)}$ equilibrium for quartz, fluorapatite, calcite, dolomite, hematite and magnetite. As expected, based on previous literature, the predicted difference between the $\delta'^{18}O$ values of quartz and liquid water is the greatest, followed by dolomite, calcite, fluorapatite hematite and magnetite. A previous experimental study has found only small fractionations for oxygen isotopes between hematite and water at surface temperatures (Bao and Koch, 1999) which is in rough agreement with the new theoretical results presented here. Comparisons of the $\Delta\delta'^{18}O$ values with previous literature are provided in the supplemental information. Similar to the $\Delta\delta'^{18}O$ trends between minerals, $\Delta\Delta'^{17}O$ values are greatest for quartz and liquid water, followed by dolomite, calcite, fluorapatite hematite and magnetite.

Analytical precisions for $\Delta'^{17}O$ have recently been significantly improved due to newly adopted methods of sample processing and purification. For silicates and most simple oxides, laser fluorination using $BrF_5$ vapor or $F_2$ gas is the preferred technique as it can generate 100% yield of $O_2$ from the sample. Purification of this $O_2$ to remove $NF_3$ and other contaminants coupled with analysis on modern mass spectrometers has allowed workers to achieve precisions of 0.005‰ for $\Delta'^{17}O$. Phosphate minerals can be

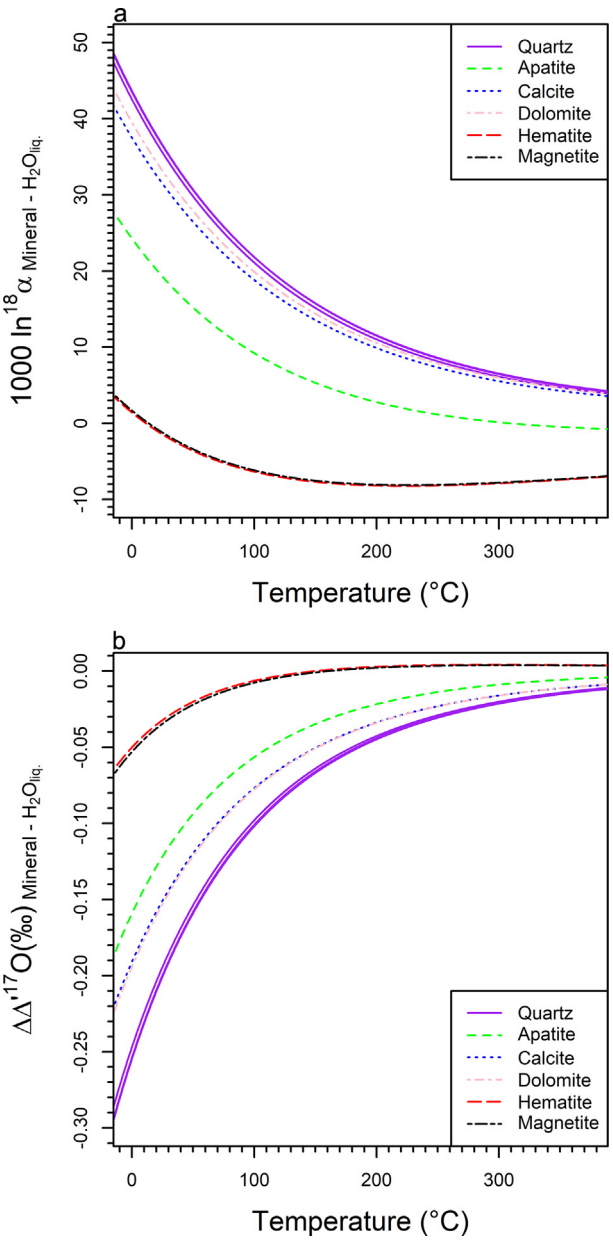


Fig. 1. Theoretical results for (a) $\Delta'\delta^{18}O$ and (b) $\Delta\Delta'^{17}O$ temperature dependence for Mineral-$H_2O_{(L)}$ equilibrium. In both figures three lines, with the larger basis set and larger cluster model lines overlapping, are plotted for quartz-water fractionation.

analyzed in the same manner as simple oxides, but give incomplete oxygen yields for fluorination. As a result, uncertainties in $\Delta'^{17}O$ from phosphate minerals are larger than for simple oxides but have been reported as low as 0.010‰ (Pack et al., 2013). For carbonates, the most accurate method to date is to convert to $CO_2$ using phosphoric acid digestion, the $CO_2$ is then reacted with hydrogen gas to generate methane and water vapor, and resulting water vapor is then reacted with $CoF_3$ to yield $O_2$ which is then purified and analyzed with a precision within ±0.01‰ (Passey et al., 2014). Because the $\Delta\Delta'^{17}O$-Temperature curve is approximately linear on the scale of these analytical uncertainties, the uncertainty of temperature determined using the $\Delta'^{17}O$ alone can be estimated by simply multiplying the analytical uncertainty by the derivative of $\Delta\Delta'^{17}O$ with respect to temperature assuming that the $\Delta'^{17}O$ of water can be constrained with a greater accuracy than analytical uncertainty. For this idealized scenario, the pure $\Delta'^{17}O$ carbonate and phosphate mineral thermometers yield an uncertainty of about ±8 °C for minerals precipitated at equilibrium near 25 °C and larger uncertainties of about ±20 °C for minerals precipitated at equilibrium near 100 °C. For quartz-$H_2O_{(L)}$, the higher precision for analysis combined with the greater temperature dependence of the triple isotope effect allows for precisions of ±3 °C for minerals precipitated at equilibrium near 25 °C and ±7 °C for minerals precipitated at equilibrium near 100 °C. This result makes the quartz-$H_2O_{(L)}$ pair the most promising of the triple isotope geothermometers. For marine environments, this would most likely find an appropriate usage with opals and cherts.

### 4.2. Comparison of Quartz- $H_2O_{(L)}$ model to previous literature

Fractionation curves for triple isotope relationships are rare in the literature at this time. The most robust work to date on the triple isotope fractionation relationship for a mineral-water system is the work of Sharp et al. (2016) which provided a calibration for the triple isotope silica-water thermometer based on measurements of natural samples of quartz, amorphous silica sinter and diatoms (opaline silica). Using results from previous work as well as new samples with temperature constraint, Sharp et al. (2016) calculated a curve for silica-water $^{18}O/^{16}O$ fractionation as a function of temperature. There is an agreement to better than 1‰ between all of our theoretical predictions for quartz-$H_2O_{(L)}$ equilibrium here and the results of Sharp et al. (2016) for $^{18}O/^{16}O$. Fig. 2 shows a comparison our new theoretical results for quartz-water equilibrium with the results of Sharp et al. (2016) as well as curves from Zheng (1993), Sharp and Kirschner (1994), and Meheut et al. (2007). Additional plots of the comparisons of the $^{18}O/^{16}O$ fractionation results of this study to literature for fluorapatite, calcite, magnetite and hematite can be found in the Supplementary Information.

The $\Delta\Delta'^{17}O_{SiO_2-H_2O_{(liq.)}}$ values from the work of Sharp et al. (2016) are close to but more negative than the theoretical calibration presented here by <0.03‰ with better agreement at higher temperatures (See Fig. 3). The reason for this discrepancy could be related to kinetic isotope fractionations or, in part, vital effects and slight differences between the $SiO_2$-$H_2O_{(L)}$ fractionation for opaline silica and quartz.

### 4.3. The triple oxygen isotope thermometer

If a mineral is in equilibrium with water with respect to $\delta^{18}O$ then it must also be in equilibrium with respect to $\Delta'^{17}O$. In one view, the triple oxygen isotope composition gives two "pure" geothermometers based on different parameters, $\delta^{18}O$ and $\Delta'^{17}O$. Similarly to the $\delta^{18}O$ based mineral-water geothermometer, a pure thermometer based

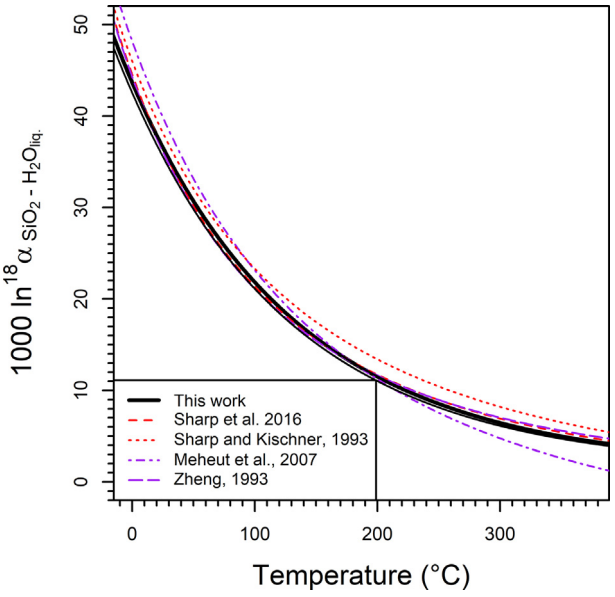


Fig. 2. Theoretical results for 1000ln($^{18}\alpha$)-temperature dependence for Quartz-H2O$_{(L)}$ equilibrium (black solid lines) with the mostly experimental curves (red dotted lines) from Sharp et al. (2016) and Sharp and Kirschner (1994) as well as a theoretical curve (purple dashed lines) from Meheut et al. (2007) and a theoretical curve assembled from previous literature by Zheng (1993). The new theoretical results are a near exact fit to the results given by Sharp et al. (2016) and Zheng (1993). (For interpretation of the references to colour in this figure legend, the reader is referred to the web version of this article.)

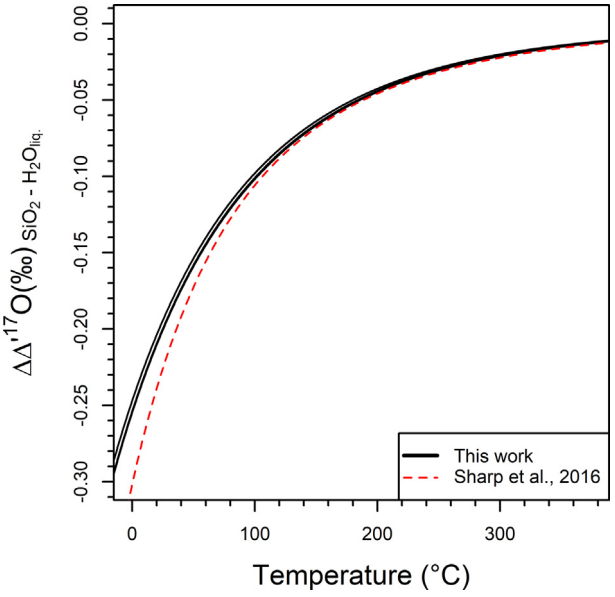


Fig. 3. Theoretical results for $\Delta\Delta'^{17}$O-temperature dependence for the three new Quartz-H2O$_{(L)}$ equilibrium models (Black solid lines) with the empirical curve from Sharp et al. (2016) (red dotted line). (For interpretation of the references to colour in this figure legend, the reader is referred to the web version of this article.)

on $\Delta'^{17}$O requires knowledge or assumptions on the $\Delta'^{17}$O of the water that the mineral precipitates from. However, because these two pure geothermometers are linked through equilibrium by a common parameter of temperature, when $\delta^{18}$O and $\Delta'^{17}$O compositions are used together it is possible that the system of equations can be solved by the assumption or knowledge of the **relationship** between $\delta^{18}$O and $\Delta'^{17}$O rather than the absolute values themselves with the degree of constraint being limited by the precisions described above for the pure $\Delta'^{17}$O geothermometer. In cases where the assumption of equilibrium holds true, there is a solution to the system of equations allowing for the calculation of both the $\delta^{18}$O and temperature of the water the mineral was in equilibrium with. This relationship between the parameters is in many cases, easier to know *a priori*, (e.g. modern meteoric water), or may be calculated in the future (e.g. ancient seawater). This makes an understanding of the relationship between $\delta^{18}$O and $\Delta'^{17}$O critical for the future utility of the triple oxygen isotope thermometer.

As the most geologically significant water reservoir, the potential for variability of the $\delta^{18}$O of seawater has been an important topic of study but little has been determined about the variability of the $\Delta'^{17}$O of seawater. Pack and Herwartz (2014) argued that the triple isotope composition of seawater should not be constant through geologic time since it is controlled by two dominant processes (1) low temperature mineral interaction during chemical weathering, which should in concept include terrestrial weathering and (2) high temperature hydrothermal exchanges. In both cases, seawater is assumed to be interacting with minerals with a composition similar to MORB glass ($\delta^{18}O = 5.60‰$; $\Delta'^{17}O = -0.05‰$) (Pack and Herwartz, 2014; Pack et al., 2016). It is argued that high temperature exchanges would have a higher value of θ (assumed 0.527) and will lead to higher seawater $\delta^{18}$O values and that the low temperature exchanges would have a lower value of θ (assumed 0.523) and will lead to lower seawater $\delta^{18}$O (Pack and Herwartz, 2014). The expectation of high θ values for high temperature processes and low θ can be justified theoretically in a general, but not absolute, way (Cao and Liu, 2011; Hayles et al., 2017). As a result of these two general processes, the triple oxygen isotope composition of seawater at any given time exists in a steady state dictated by the relative contributions of high and low temperature mineral-water interactions. Although this is a simple model representing a truly complex system, it is a first step toward determining the history of seawater $\Delta'^{17}$O.

For meteoric waters, $\Delta'^{17}$O is determined by equilibrium between liquid water and vapor, the kinetic isotope effect contribution to evaporation which is a function of relative humidity, the effects of Rayleigh distillation and the isotope composition of seawater (Bao et al., 2016). Generally this leads to the relationship $\Delta\delta'^{17}O = 0.528\ \Delta\delta'^{18}O$ for the average comparison of any two meteoric waters with meteoric waters having a higher $\Delta'^{17}$O value than seawater relative to VSMOW. This relationship is valid for the modern Earth system but is expected to be a function of global climate conditions. A dominant factor controlling the $\Delta'^{17}$O of meteoric waters is the $\Delta'^{17}$O of seawater for that time.

The history of the triple isotope composition of seawater is therefore a critical unknown needed for the future application of the triple oxygen isotope geothermometer.

## 5. CONCLUSION

Theoretical calibrations for several geologically important mineral-water triple isotope equilibrium thermometers can be done by utilizing well developed quantum chemical methods combined with a semi-empirical approach to model liquid water. The results presented here compare well with previous for $^{18}O/^{16}O$ fractionation where data is available. Of the models given here, pairs of quartz, calcite, dolomite and fluorapatite with water show promise as triple isotope thermometers with acceptable uncertainties for Earth surface and low-T hydrothermal environments.

There is a critical need to determine the history of seawater $\Delta'^{17}O$ on geological timescales. The calibrations provided here with appropriate marine samples, make this possible. The process of determining the history of seawater $\Delta'^{17}O$ using the presented calibrations will result in a history of seawater $\delta'^{18}O$ that is better constrained and more reliable than when using two isotope techniques alone.

## ACKNOWLEDGEMENTS

We appreciate discussions with Laurence Yeung. Financial support is provided by the strategic priority research program (B) of CAS (XDB18010104), US NSF grant EAR-1251824, and China NSFC grant 41490635 to HB.

## APPENDIX A. SUPPLEMENTARY MATERIAL

Supplementary data associated with this article can be found, in the online version, at https://doi.org/10.1016/j.gca.2018.05.032.

## REFERENCES

Bao H. M., Cao X. B. and Hayles J. (2016) Triple oxygen isotopes: fundamental relationships and applications. *Annu. Rev. Earth Planet. Sci.* **44**.

Bao H. M. and Koch P. L. (1999) Oxygen isotope fractionation in ferric oxide-water systems: Low temperature synthesis. *Geochim. Et Cosmochim. Acta* **63**, 599–613.

Barkan E. and Luz B. (2005) High precision measurements of $^{17}O/^{16}O$ and $^{18}O/^{16}O$ ratios in $H_2O$. *Rapid Commun. Mass Spectrom.* **19**, 3737–3742.

Bigeleisen J. and Goeppert-Mayer M. (1947) Calculation of equilibrium constants for isotopic exchange reactions. *J. Chem. Phys.* **15**, 261–267.

Cao X. B. and Liu Y. (2011) Equilibrium mass-dependent fractionation relationships for triple oxygen isotopes. *Geochim. Et Cosmochim. Acta* **75**, 7435–7445.

Clayton R. N., Grossman L. and Mayeda T. K. (1973) Component of primitive nuclear composition in carbonaceous meteorites. *Science* **182**, 485–488.

Downs R. T. and Hall-Wallace M. (2003) The American mineralogist crystal structure database. *Am. Mineral.*, 247–250.

Driesner T. and Seward T. M. (2000) Experimental and simulation study of salt effects and pressure/density effects on oxygen and hydrogen stable isotope liquid-vapor fractionation for 4–5 molal aqueous NaCl and KCl solutions to 400 °C. *Geochim. Cosmochim. Acta* **64**, 1773–1784.

Frisch M. J., Trucks G. W., Schlegel H. B., Scuseria G. E., Robb M. A., Cheeseman J. R., Scalmani G., Barone V., Mennucci B., Petersson G. A., Nakatsuji H., Caricato M., Li X., Hratchian H. P., Izmaylov A. F., Bloino J., Zheng G., Sonnenberg J. L., Hada M., Ehara M., Toyota K., Fukuda R., Hasegawa J., Ishida M., Nakajima T., Honda Y., Kitao O., Nakai H., Vreven T., Montgomery, Jr., J. A., Peralta J. E., Ogliaro F., Bearpark M., Heyd J. J., Brothers E., Kudin K. N., Staroverov V. N., Keith T., Kobayashi R., Normand J., Raghavachari K., Rendell A., Burant J. C., Iyengar S. S., Tomasi J., Cossi M., Rega N., Millam J. M., Klene M., Knox J. E., Cross J. B., Bakken V., Adamo C., Jaramillo J., Gomperts R., Stratmann R. E., Yazyev O., Austin A. J., Cammi R., Pomelli C., Ochterski J. W., Martin R. L., Morokuma K., Zakrzewski V. G., Voth G. A., Salvador P., Dannenberg J. J., Dapprich S., Daniels A. D., Farkas O., Foresman J. B., Ortiz J. V., Cioslowski J. and Fox D. J. (2016) *Gaussian 09, Revision D.01*. Gaussian, Inc., Wallingford CT.

Gibbs G. V. (1982) Molecules as models for bonding in silicates. *Am. Mineral.* **67**, 421–450.

Hayles J. A., Cao X. and Bao H. (2017) The statistical mechanical basis of the triple isotope fractionation relationship. *Geochem. Perspect. Lett.* **3**, 1–11.

Heidenreich J. E. and Thiemens M. H. (1983) A non-mass-dependent isotope effect in the production of ozone from molecular-oxygen. *J. Chem. Phys.* **78**, 892–895.

Hill P. S., Tripati A. K. and Schauble E. A. (2014) Theoretical constraints on the effects of pH, salinity, and temperature on clumped isotope signatures of dissolved inorganic carbon species and precipitating carbonate minerals. *Geochim. Cosmochim. Acta* **125**, 610–652.

Horita J., Rozanski K. and Cohen S. (2008) Isotope effects in the evaporation of water: a status report of the Craig-Gordon model. *Isotopes Environ. Health Stud.* **44**, 23–49.

Huang F., Chen L. J., Wu Z. Q. and Wang W. (2013) First-principles calculations of equilibrium Mg isotope fractionations between garnet, clinopyroxene, orthopyroxene, and olivine: Implications for Mg isotope thermometry. *Earth Planet. Sci. Lett.* **367**, 61–70.

Lecuyer C., Amiot R., Touzeau A. and Trotter J. (2013) Calibration of the phosphate delta O-18 thermometer with carbonate-water oxygen isotope fractionation equations. *Chem. Geol.* **347**, 217–226.

Li X. F. and Liu Y. (2015) A theoretical model of isotopic fractionation by thermal diffusion and its implementation on silicate melts. *Geochim. Cosmochim. Acta* **154**, 18–27.

Liang M.-C. and Mahata S. (2015) Oxygen anomaly in near surface carbon dioxide reveals deep stratospheric intrusion. *Scient. Rep.* **5**, 11352.

Longinel A. and Nuti S. (1973) Revised phosphate-water isotopic temperature scale. *Earth Planet. Sci. Lett.* **19**, 373–376.

Meheut M., Lazzeri M., Balan E. and Mauri F. (2007) Equilibrium isotopic fractionation in the kaolinite, quartz, water system: prediction from first-principles density-functional theory. *Geochim. Cosmochim. Acta* **71**, 3170–3181.

Pack A. and Herwartz D. (2014) The triple oxygen isotope composition of the Earth mantle and understanding Delta O-17 variations in terrestrial rocks and minerals. *Earth Planet. Sci. Lett.* **390**, 138–145.

Pack A., Gehler A. and Sussenberger A. (2013) Exploring the usability of isotopically anomalous oxygen in bones and teeth as paleo-CO2-barometer. *Geochim. Cosmochim. Acta* **102**, 306–317.

Pack A., Tanaka R., Hering M., Sengupta S., Peters S. and Nakamura E. (2016) The oxygen isotope composition of San Carlos olivine on the VSMOW2-SLAP2 scale. *Rapid Commun. Mass Spectrom.* **30**, 1495–1504.

Passey B. H., Hu H. T., Ji H. Y., Montanari S., Li S. N., Henkes G. A. and Levin N. E. (2014) Triple oxygen isotopes in biogenic and sedimentary carbonates. *Geochim. Cosmochim. Acta* **141**, 1–25.

R Core Team, 2012. R: A Language and Environment for Statistical Computing. R Foundation for Statistical Computing.

Rustad J. R., Casey W. H., Yin Q. Z., Bylaska E. J., Felmy A. R., Bogatko S. A., Jackson V. E. and Dixon D. A. (2010) Isotopic fractionation of Mg2+(aq), Ca2+(aq), and Fe2+(aq) with carbonate minerals. *Geochim. Cosmochim. Acta* **74**, 6301–6323.

Schauble E. A. (2011) First-principles estimates of equilibrium magnesium isotope fractionation in silicate, oxide, carbonate and hexaaquamagnesium(2+) crystals. *Geochim. Et Cosmochim. Acta* **75**, 844–869.

Sharp Z. D., Gibbons J. A., Maltsev O., Atudorei V., Pack A., Sengupta S., Shock E. L. and Knauth L. P. (2016) A calibration of the triple oxygen isotope fractionation in the SiO2–H2O system and applications to natural samples. *Geochim. Cosmochim. Acta* **186**, 105–119.

Sharp Z. D. and Kirschner D. L. (1994) Quartz-calcite oxygen-isotope thermometry - a calibrtion based on natural isotopic variations. *Geochim. Cosmochim. Acta* **58**, 4491–4501.

Thiemens M. H. (2013) Introduction to chemistry and applications in nature of mass independent isotope effects special feature. *Proc. Natl. Acad. Sci.* **110**, 17631–17637.

Urey H. C. (1947) The thermodynamic properties of isotopic substances. *J. Chem. Soc.*, 562–581.

Webb M. A. and Miller T. F. (2014) Position-specific and clumped stable isotope studies: comparison of the urey and path-integral approaches for carbon dioxide, nitrous oxide, methane, and propane. *J. Phys. Chem. A* **118**, 467–474.

Wiechert U. H., Halliday A. N., Palme H. and Rumble D. (2004) Oxygen isotope evidence for rapid mixing of the HED meteorite parent body. *Earth Planet. Sci. Lett.* **221**, 373–382.

Zheng Y. F. (1993) Calculation of oxygen isotope fractionation in anhydrous silicate minerals. *Geochim. Cosmochim. Acta* **57**, 1079–1091.

*Associate editor:* Ruth Blake